Astronomy & Astrophysics manuscript no. paper-arxiv
March 11, 2014
©ESO 2014

arXiv:1403.2240v1 [astro-ph.SR] 10 Mar 2014

Fundamental and harmonic plasma emission in different plasma environments
(Research Note)

U. Ganse[1], P. Kilian[2], F. Spanier[3], and R. Vainio[1,4]

[1] Department of Physics, University of Helsinki, 00014 Helsinki, Finland
[2] Max-Planck Institut für Sonnensystemforschung, 37077 Göttingen, Germany
[3] Center for Space Research, North-West University, 2520 Potchefstrom, South Africa
[4] Department of Physics and Astronomy, University of Turku, 20014 Turku, Finland

March 11, 2014

ABSTRACT

Aims. Emission of radio waves from plasmas through plasma emission with fundamental and harmonic frequencies is a familiar process known from solar type II radio bursts. Current models assume the existence of counterstreaming electron beam populations excited at shocks as sources for these emission features, which limits the plasma parameters to reasonable heliospheric shock conditions. However, situations in which counterstreaming electron beams are present can also occur with different plasma parameters, such as higher magnetisation, including but not limited to our Sun. Similar radio emissions might also occur from these situations.
Methods. We used particle-in-cell simulations, to compare plasma microphysics of radio emission processes from counterstreaming beams in different plasma environments that differed in density and magnetization.
Results. Although large differences in wave populations are evident, the emission process of type II bursts appears to be qualitatively unaffected and shows the same behaviour in all environments.

Key words. Sun: radio radiation - Waves - Plasmas

1. Introduction

Solar type II radio bursts are intermittent radio phenomena within the heliosphere that have been observed and recorded since the earliest days of astronomical radio observations (Wild & McCready 1950). These bursts, observed in conjunction with coronal mass ejections (CME) (Cane & Erickson 2005) and shocks driven by other flare-related eruptions (Liu et al. 2009; H. Aurass et al. 2002), show a characteristic multibanded spectral morphology: typically two frequency bands, called the fundamental and harmonic emission, exist at frequencies typically between 10 and 1000 MHz and are drifting towards lower frequencies at a rate of about 0.25 MHz/s (Nelson & Melrose 1985).

The emission process of these bursts arises from non-thermal electron beam populations excited through shock drift acceleration at the leading edge of the corresponding CME- or flare-driven shock (Nelson & Melrose 1985; Forbes et al. 2006; Knock et al. 2001), causing beam-driven instabilities (Mikhailovskii 1981) in the foreshock region, especially in the presence of counterstreaming electron beams caused by shock ripples (Knock et al. 2003). The resulting electrostatic wavemodes can participate in nonlinear interaction processes, thus radiating radio emission at the plasma frequency and its harmonic (Melrose 1970, 1986; Willes & Cairns 2000; Spanier & Vainio 2009):

$$L \rightarrow S + T(\omega_p) \quad (1)$$

$$L + L' \rightarrow T(2\omega_p). \quad (2)$$

Here, L and L' denote forward- and backward-propagating beam-driven Langmuir waves, S denotes ion soundwaves and T denotes transverse electromagnetic modes. These processes are depicted in Figure 1.

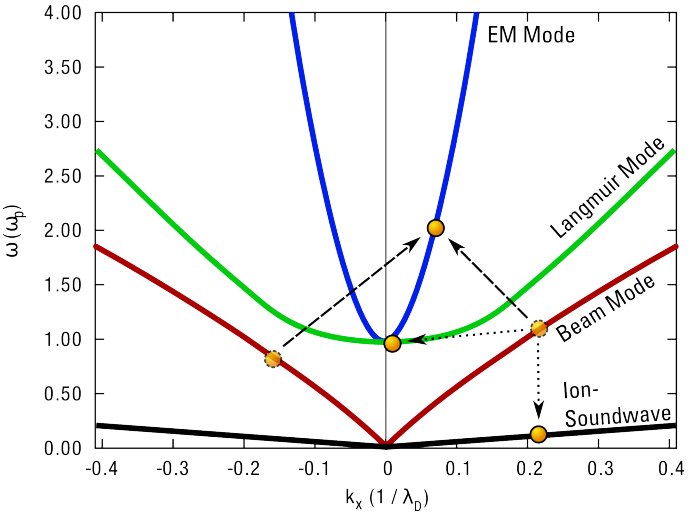

Fig. 1. Kinematics of the nonlinear wave coupling processes leading to type II radio burst emission: decay of electrostatic wave energy (dotted arrows) excites ion soundwaves and radio emissions at the plasma frequency ω_p, while coalescence of counter-propagating electrostatic waves (dashed arrows) creates radio emissions at $2\omega_p$

.

Remote verification of the nonlinear interaction processes through radio observations is hampered by the fact that nonlin-

Send offprint requests to: U. Ganse, e-mail: urs.ganse@helsinki.fi

ear plasma excitations can only leave the emission regions where they couple to propagating linear modes - in this case, where the nonlinear excitations are coincident with the electromagnetic modes' dispersion relation. These are detectable as the familiar fundamental and harmonic frequency bands of type II radio bursts, which do not, by themselves, carry any information about the k-space distribution of the nonlinear processes that originally excited them.

Even in scarce in situ spacecraft observations of radio burst emission regions (Pulupa & Bale 2008), only partial information about the wave populations present there are obtainable, since the pointwise measurement of wave spectrometers can only provide ω but no k information. Only in computer simulations can complete spatiotemporal information on any wave quantity be obtained.

In previous works, the authors have investigated the processes in this emission region using a particle-in-cell simulation model (Kilian et al. 2012; Hockney & Eastwood 1988): the dependence of the emission intensity on the beam strength has been probed by Ganse et al. (2012a) and uni- versus bidirectional electron beams have been compared by Ganse et al. (2012b).

Because they are directly produced via nonlinear plasma processes near a coronal shock front (Knock et al. 2003), the plasma environments are constrained by conditions under which shock-formation is possible – specifically, the magnetic field strength and consequently the Alfvén velocity has to be low enough for super-Alfvénic velocities to be achieved by solar ejecta. Thus, an effective upper limit for the Alfvén velocity at shocks of about 2000 km/s exists. In a CME's loop structure, however, no such limitation exists and counterstreaming beam situations can potentially occur in much stronger magnetic fields, caused for example by magnetic bottle configurations. These environments are not constrained to small spatial extents and heliospheric-shock magnetic field strengths, so emissions from these regions can be assumed to be broadband in nature. In a recent study by Pohjolainen et al. (2013), a number of wideband type II radio burst events are shown to propagate slower than the shock they are associated with, which might be another indication that the emission process is not necessarily confined to the foreshock region and that a continuum of phenomena between type II and type IV bursts may exist.

In addition to at the Sun, radio bursts have also been observed for nearby flare stars (Osten & Bastian 2008), where higher densities and magnetic fields are also implied.

The open question in this model is whether the three-wave interaction processes confirmed to take place at low magnetic field strengths can equally contribute to radio emissions from areas where magnetic fields are significantly stronger, or whether synchrotron radiation is the only viable emission mechanism.

Whereas theoretical treatment of type II bursts (Melrose 1986) is typically based on the assumption of only one electromagnetic mode being present in the emitting medium, splitting into R- and L-mode (for field-parallel propagation) or X- and O-mode (for propagation perpendicular to the magnetic field) can potentially alter the interaction behaviour.

Therefore, by varying the simulation setup in plasma density and magnetisation, the viability of the same emission process for broadband type II/IV radio bursts is tested here.

Setup

Simulations were performed using the ACRONYM particle-in-cell code (Kilian et al. 2012), a fully relativistic electromagnetic code tuned for the study of kinetic-scale plasma wave phenomena and -interactions. The simulation setup was adopted from the previous works (Ganse et al. 2012a,b), with a spatially periodic, 2.5-dimensional simulation box filled with a homogeneous plasma, into which two counterstreaming non-thermal beam components were injected at $v_{\mathrm{beam}} \approx 5\, v_{\mathrm{th}}$.

Table 1. Simulation parameters of the three particle-in-cell simulation runs.

#	**Simulation size**/cells	$\mathbf{B_0}$/G	ρ_{e} /cm^{-3}	Ω_{ce}/ω_{pe}
1	8192×4096	1	$1.25 \cdot 10^7$	0.093
2	4096×4096	0.015	$1.05 \cdot 10^2$	0.689
3	4096×4096	0.22	$3.06 \cdot 10^3$	1.729

Simulation #1 used parameters based on observations of foreshock plasmas, with weak magnetization and coronal density. For simulation #2 and #3, the ratio of electron gyro frequency to plasma frequency was subsequently increased as denoted in Table 1, thus representing plasma environments with correspondingly stronger magnetization. (It should be noted that both plasma density and magnetic field strength are actually decreasing in the simulation parameters. However, the particle-in-cell simulation method allows arbitrary rescaling with respect to plasma frequency, so the results are valid for all plasmas of the given frequency ratio.)

The corresponding change in Debye length, gyroradius, and plasma frequency resulted in appropriately larger physical extents of the simulation, which were all run at roughly the same numerical resolution. We note that the particle distribution in velocity space remained unchanged between all three runs, meaning that all simulations were run with the same thermal and electron beam velocities.

Results

To investigate the predicted nonlinear wave couplings, both electrostatic and electromagnetic wave behaviour have to be analyzed. The simplest quantity for assessing their respective intensities is the total energy content of longitudinal electric fields (as a measurement of electrostatic waves) and the transverse magnetic field energy (as a measurement of magnetic field intensity), integrated over the complete simulation box. Figure 2 shows the development of these quantities over the time span of the simulation runs. The electric field energy initially rises strongly, as beam-driven wave excitation forms the electrostatic wave population. This process eventually saturates, as sufficient kinetic energy of the beam electrons is depleted. Correspondingly, the transverse magnetic energy shows a much slower start of its growth, consistent with the nonlinear excitation from electrostatic wavemode couplings.

It is apparent that this behaviour is represented identically in all three simulation runs, with their relative energy densities scaled by the changing plasma density and spatial extent of the simulations.

For a more detailed comparison of the individual wavemodes, the field quantities within the simulation were spatially and temporally Fourier-transformed to obtain intensities in $k - \omega$ space, which allows for direct identification of wavemodes through their characteristic dispersion relations. Figure 3 shows the dispersion behaviour of the longitudinal electric field so obtained for each of the three simulation runs. A total change in intensity due to plasma parameter rescaling based on density again is the only change visible in these plots – no morpholog-

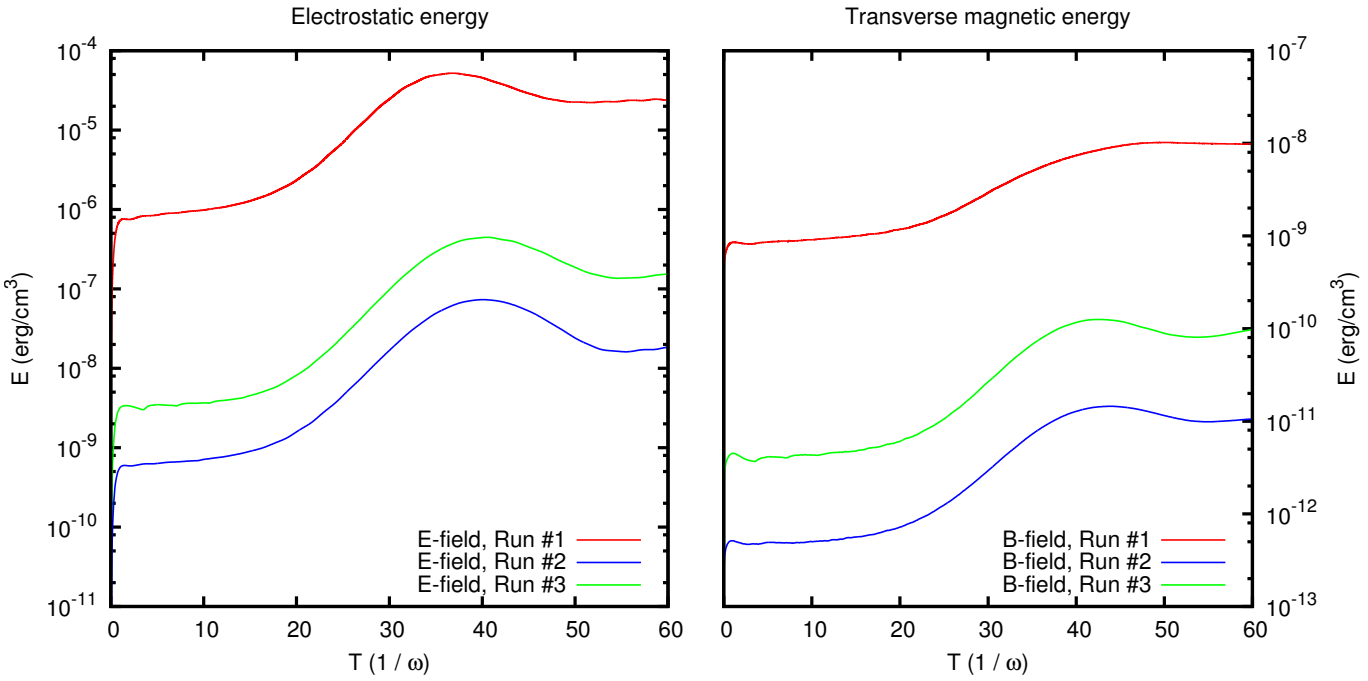

Fig. 2. Distribution of electric field (as a measure of electrostatic wave intensity) and transverse magnetic field strength (as a measure of electromagnetic wave intensity) in simulation runs #1, #2 and #3, shown in red, blue and green.

ical change of wave excitation can be observed. The dominant wave feature in all three plots is the beam-driven wave, whose dispersion forms a linear feature with a slope corresponding to the electron beam velocity. The strongest excitation occurs in resonance with the electron plasma frequency ω_p, as predicted by Mikhailovskii (1981) and Willes & Cairns (2000).

More interestingly, the dispersion behaviour of a transverse magnetic field component in all three simulations is given in Figure 4, which show the spatial and temporal Fourier transform of a transverse component of the magnetic field. Transform direction was chosen along the background field (for simulations #1 and #3) or orthogonal to it (for simulation #2). Here, the effect of changing magnetisation is clearly visible in the changed mode composition between the three simulations: while simulation #1 shows an electromagnetic mode that is nearly undisturbed by the background magnetic field, the splitting into X- and O-mode is becoming apparent in simulation #2 and very pronounced splitting into R- and L-mode in case #3. Still, common to all three simulation runs are horizontal emission bands at the fundamental (ω_p) and harmonic ($2\omega_p$) frequency, which do not correspond to any linear wave mode of the plasma. These features have previously been identified (Ganse et al. 2012a; Karlický & Barta 2010) as the predicted nonlinear excitations caused by interaction of beam-driven modes and Langmuir waves. Observationally, these bands correspond to the radio excitations at ω_p and $2\omega_p$, identified as the fundamental and harmonic frequency bands of type II radio bursts.

Because they are a product of electrostatic waves, these features appear to be largely unaffected by the change in magnetisation, and are consistently occurring in all plasma environments investigated here. By coupling to the electromagnetic mode, in whatever configuration it may be present within the emission region, the nonlinear process can thus lead to radio emission at the fundamental and harmonic frequency.

To further investigate the development of energies contained in the fundamental and harmonic emission bands, the latter half ($t > 20/\omega_p$) of the simulation was divided into a number of temporal subdivisions, and dispersion analysis was run individually for each of the slices. Because time and frequency are conjugated quantities, a reduction in temporal extent leads to a reduction in frequency resolution in these dispersion snapshots. Hence, as a compromise between sufficient temporal and spectral resolution, the times were chosen such that both fundamental and harmonic emission bands remained clearly discernable in the plots, leading to five data points for simulation #1 and #3, and three data points for simulation #2.

By summing over the intensities contained in these bands, we determined the mode intensity development. Figure 5 shows the resulting individual behaviour in the latter half of the simulations. In all three cases, both modes follow the total energy development of the transverse magnetic fields. While simulations #1 and #3 show more energy in the fundamental than in the harmonic emission band, the reverse is true for simulation #2. The close proximity of the electron cyclotron frequency to the harmonic band's frequency is assumed to be the culprit here – in the dispersion diagrams, the lack of a clear separation between R-mode and nonlinear harmonic excitation causes both to contribute to the measured mode intensity.

Conclusion

Through 2.5D particle-in-cell simulations, we have investigated the excitation of electrostatic waves in heliospheric plasmas and their subsequent coupling to nonlinearly create electromagnetic waves, known from type II radio bursts, focusing on the question whether the emission process of these bursts is significantly affected by the emission regions' background magnetic field strength.

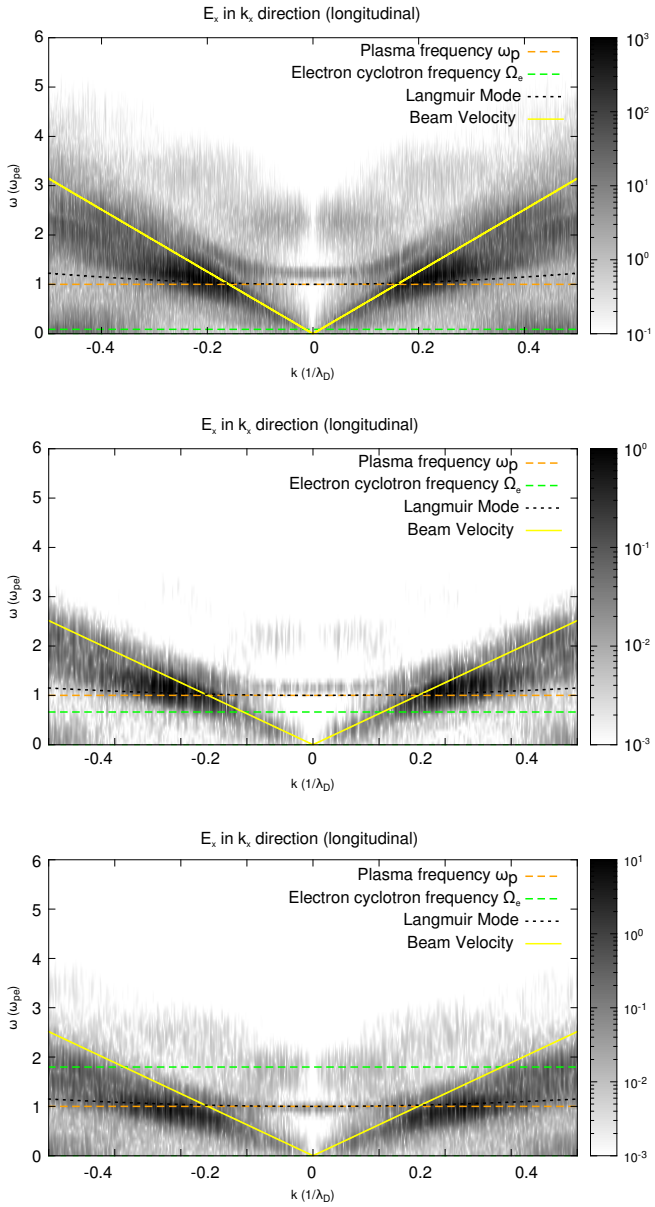

Fig. 3. Comparison of electrostatic wave dispersion and intensities for simulations with increasing magnetization. Apart from intensity rescaling due to different plasma densities, no morphological changes in wave behaviour occur.

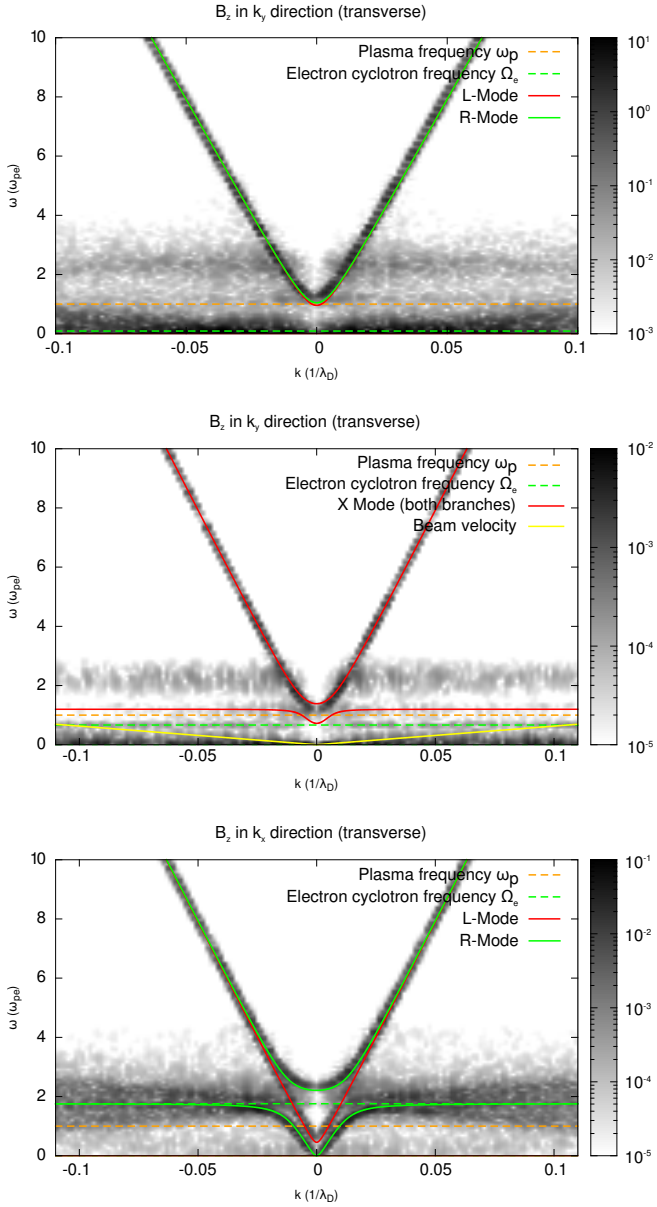

Fig. 4. Comparison of electromagnetic wave dispersion and intensities for simulations with different magnetization strengths: #1 (top) #2 (centre) and #3 (bottom). While the spectral structure of electromagnetic modes varies strongly between the three runs, the horizontal bands of nonlinear wave excitation persist regardless of magnetic field strength.

Results show that the electrostatic wave excitation is unaffected by the strong changes in plasma magnetisation, and creates self-consistent wave populations at all studied ratios of electron cyclotron frequency to plasma frequency. The subsequent nonlinear coupling of electrostatic modes causes emission features to appear at both the fundamental (ω_p) and harmonic ($2\omega_p$) frequency, these processes, too, occur irrespective of magnetization. Even though the electromagnetic modes' dispersion behaviour changes drastically at higher magnetizations, the excitation process can thus consistently drive radio emissions with the same spectral properties and lead to the observed continuous emission of type II radio bursts during propagation of coronal shocks over a wide range of solar radii.

The same emission process may therefore be responsible for other heliospheric radio emission phenomena, such as broadband type II or type IV bursts, whose assumed emission regions may contain counterstreaming electron populations at much higher magnetic fields. It is also a viable emission mechanism for highly magnetized flare stars.

In a direct comparison of the development of fundamental and harmonic emission intensity it became apparent that the harmonic emission was significantly enhanced in the case where the electron cyclotron frequency was approximately resonant. In which way these wave resonances may have a quantitative effect on actual radio observations will have to be determined in a future study.

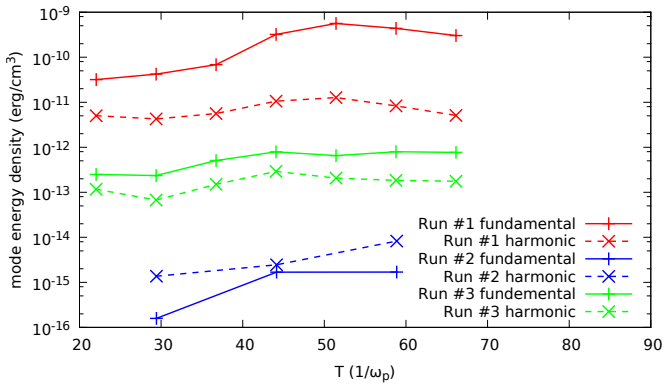

Fig. 5. Development of harmonic and fundamental mode energies in the second half of the simulation (where a sufficiently strong signal was discernible).

Acknowledgements

The Academy of Finland is acknowledged for financial support (Project 133723). The simulations for this research have been made possible through computing grants by the Juelich Supercomputing Centre (JSC) and the CSC - IT Center for Science Ltd., Espoo, Finland. This work has been supported by the European Framework Programme 7 Grant Agreement SEPServer - 262773

References

Cane, H. V. & Erickson, W. C. 2005, The Astrophysical Journal, 623, 1180
Forbes, T., Linker, J., Chen, J., et al. 2006, Space Science Reviews, 123, 251
Ganse, U., Kilian, P., Spanier, F., & Vainio, R. 2012a, ApJ, 751, 145(6pp)
Ganse, U., Kilian, P., Vainio, R., & Spanier, F. 2012b, Solar Physics, 280, 551
H. Aurass, B. Vrsnak, & G. Mann. 2002, A&A, 384, 273
Hockney, R. W. & Eastwood, J. W. 1988, Computer simulation using particles (Bristol: Hilger, 1988)
Karlický, M. & Barta, M. 2010, Proceedings of the International Astronomical Union, 6, 252
Kilian, P., Burkart, T., & Spanier, F. 2012, in High Performance Computing in Science and Engineering '11, ed. W. E. Nagel, D. B. Kröner, & M. M. Resch (Berlin Heidelberg: Springer), 5–13
Knock, S. A., Cairns, I. H., & Robinson, P. A. 2003, J. Geophys. Res., 108, 1361
Knock, S. A., Cairns, I. H., Robinson, P. A., & Kuncic, Z. 2001, Journal of Geophysical Research, 106, 25041
Liu, Y., Luhmann, J. G., Bale, S. D., , & Lin, R. P. 2009, The Astrophysical Journal Letters, 691, L151
Melrose, D. B. 1970, Australian Journal of Physics, 23, 871
Melrose, D. B. 1986, Instabilities in Space and Laboratory Plasmas (Instabilities in Space and Laboratory Plasmas, by D. B. Melrose, pp. 288. ISBN 0521305411. Cambridge, UK: Cambridge University Press)
Mikhailovskii, A. B. 1981, Plasma Physics, 23, 413
Nelson, G. J. & Melrose, D. B. 1985, Type II bursts (Cambridge University Press), 333–359
Osten, R. A. & Bastian, T. S. 2008, ApJ, 674, 1078
Pohjolainen, S., Allawi, H., & Valtonen, E. 2013, A&A, 558, A7
Pulupa, M. & Bale, S. D. 2008, The Astrophysical Journal, 676, 1330
Spanier, F. & Vainio, R. 2009, Advanced Science Letters, 2, 337
Wild, J. & McCready, L. 1950, Australian Journal of Scientific Research, 3, 387
Willes, A. J. & Cairns, I. H. 2000, Physics of Plasmas, 7, 3167